Article

Effect of Orange Fruit Peel Extract Concentration on the Synthesis of Zinc Oxide Nanoparticles

Getachew Tizazu * and Emebet Wondimu

Posted Date: 10 June 2024

doi: 10.20944/preprints202405.0630.v2

Keywords: zinc oxide; nanoparticle; reducing agent; surface energy; band gap and size of zinc oxide nanoparticles

Article

Effect of Orange Fruit Peel Extract Concentration on the Synthesis of Zinc Oxide Nanoparticles

Emebet Wondimu and Getachew Tizazu *

Department of Physics, Bahir Dar University, Bahir Dar, Ethiopia
* Correspondence: getachewtizazu@gmail.com

Abstract: In this investigation, the impact of reducing agent concentration on the synthesis of zinc oxide nanoparticles was examined. During the synthesis, an assessment of ionic conductivity was carried out, revealing a significant increase in conductivity prior to the introduction of the reducing agent, followed by a sharp decrease upon its addition. Characterization of the ZnO NPs involved UV-visible spectroscopy, scanning electron microscopy, Fourier Infrared Spectroscopy, and X-Ray Diffraction analysis. The outcomes suggest that the characteristics of the ZnO NPs are influenced by the concentration of the reducing agent during the synthesis process. Notably, the ZnO NPs synthesized with a higher concentration of reducing agent exhibited a narrower optical band gap and increased surface energy. Furthermore, employing a concentration of 0.5 v/v resulted in the rapid production of nanoparticles with relatively uniform sizes. Conversely, concentrations below 0.5 v/v lead to slow formation, while concentrations exceeding 0.5 v/v yielded non-uniform nanoparticles.

Keywords: zinc oxide; nanoparticle; reducing agent; surface energy; band gap and size of zinc oxide nanoparticles

1. Introduction

Metal oxide nanoparticles can be synthesized using environmentally friendly reducing agents such as plant extracts [1]. These methods are nowadays more preferred than chemical and physical methods because they are non-toxic and less costly [2]. There are studies on the effect of the reducing agent concentration on the size and shape of metal nanoparticles. Rajalakshmi et al. studied the effect of the concentration of Impatiens balsamina L. plant flower extract (utilized as a reducing agent) on the synthesis of silver nanoparticles and observed that high concentration of extract led to the production of smaller nanoparticles [3]. Similarly, Kim et al. explored variations in reducing agent concentration during the synthesis of gold nanoparticles. Their findings indicated that an increase in reducing agent concentration resulted in a reduction in the size of AuNPs, [4]. Despite the prevalent preference for green synthesis over chemical methods, there is a notable absence of comparative research on the effects of reducing agent concentration on the characteristics of zinc oxide nanoparticles (ZnO NPs) in existing literature. Therefore, in this paper, we studied the effect of reducing agent concentration on the size of ZnO NPs, which are one of the most widely used metal oxide nanoparticles for device fabrication and preparation of beauty products [5]. In the investigation, SEM analysis was used to confirm shape and size, and EDX was utilized to check the purity and composition of the NPs. FTIR was employed to examine the stretching and bonding, X-Ray Diffraction was used to investigate the structure and average size, and UV-vis was utilized to study the optical properties of the ZnO NPs.

2. Materials and Methods

Zinc oxide nanoparticles were synthesized by employing various concentrations of orange peel extract as a reducing agent. Following this, the absorption spectra of the samples were measured using a UV-Vis spectrometer (DR6000 model, Germany). The band gap energy of the ZnO nanoparticles was determined from the UV-visible spectra using the Tauc plot methodology [6].

 doi:10.20944/preprints202405.0630.v2

Additionally, the nanoparticle size of ZnO was calculated based on the band gap utilizing the effective mass model (Equation 1) [7].

$$r = \frac{2A}{-B+\sqrt{B^2+4AC}} \quad \text{Where } A = \frac{h^2}{8m_0e^2}\left(\frac{1}{m_e^*}+\frac{1}{m_h^*}\right),\ B = -\frac{1.8e^2}{4\pi\varepsilon\varepsilon_0},\ C = E_g^{bulk} - E_g^* - \frac{0.124e^3m_0}{h^2(2\varepsilon\varepsilon_0)^2}\left(\frac{1}{m_e^*}+\frac{1}{m_h^*}\right)^{-1} \quad \ldots.1$$

Where, E_g^{Bulk} is the bulk band gap of ZnO (3.2eV)[8], h $=6.625\times10^{-34}$ J·s , r is particle radius (m), m_o is the free electron mass (9.11×10^{-31} kg), m_e^* is effective mass of an electron (0.24 m_o), m_h^* is effective mass of the hole (0.45m_o), e is the charge on an electron(1.602×10^{-19}C), ε_0 is the permittivity of free space (8.85x10^{-12} C^2 m^{-2}), and ε is relative permittivity (3.7)[3]. Additionally, the concentration of the nanoparticles was determined using the Beer-Lambert law, $A = \alpha cl$, where A is absorbance, α is the molar extinction coefficient with unit of M^{-1} cm^{-1}, l is the path length of the sample (1 cm), and c is the number of suspensions of ZnO NPs (M)[9]. The FT-IR spectra were recorded using a Perkin Elmer spectrum two spectrometer. The XRD patterns were acquired by X-Ray Diffractometer (XRD-6000, Shimadzu, Japan) using Cu Kα radiation (λ = 0.15406175 nm). Based on the XRD data, the crystalline size of the ZnO NPs was obtained using the Debye-Scherer equation $D = \frac{K\lambda}{\beta\cos\theta'}$, where, D is the average size of the crystalline, λ is the wavelength of the X-ray (0.15406175 nm), k is the shape factor or Scherer's constant (0.94), θ is Bragg's diffraction angle, and β is the full width of the XRD peak at half maximum[10]. Besides, after the determination of the crystal structure using XRD and the determination of the size from the energy gap, the surface energy of the ZnO NPs , $\gamma_{nano} = \gamma_0\left(1-\frac{r_o}{r}\right)^2$, can be readily calculated based on the size (r), bond energy , and lattice constants of the unit cell[11]. Moreover, the morphology and particle size were studied using a scanning electron microscope (JEOL JSM-6701F) and the elemental composition was determined using an energy dispersive X-Ray Spectrometer (ZEISS SIGMA). The thermal stability was analyzed by thermogravimetric analysis (BJHENVEN, HCT-1).

3. Result and Discussions

Figure 1a shows the variation in the conductivity of the ZnO NPs' forming solution over time. Initially, there was a sharp increase in conductivity that was attributed to the dissolution of the precursor, leading to an increase in the number of ions in the solution. Subsequently, a plateau in conductivity was observed between 5 and 60 seconds, indicating complete dissolution of all precursors with no further ion addition. In the final stage, a decrease in conductivity was noted because of the introduction of a reducing agent, which facilitated the reduction of ions to neutral nanoparticle forming atoms. Figure 1b illustrates the UV–vis absorbance spectra of ZnO NPs fabricated using varying concentrations of orange peel extract (0.25 v/v, 0.35 v/v, 0.5 v/v, and 1 v/v). The shift in peak wavelength toward longer wavelengths as the concentration of the orange peel extract increases is attributed to the increased availability of electron donors at a higher concentration of the reducing agent. These electron donors aid in the reduction of precursor ions into their corresponding neutral atoms. Figure 1c is the Tauc plot of the ZnO NPs synthesized using a concentration of 0.25 v/v orange peel extract and the band gap is 3.37.

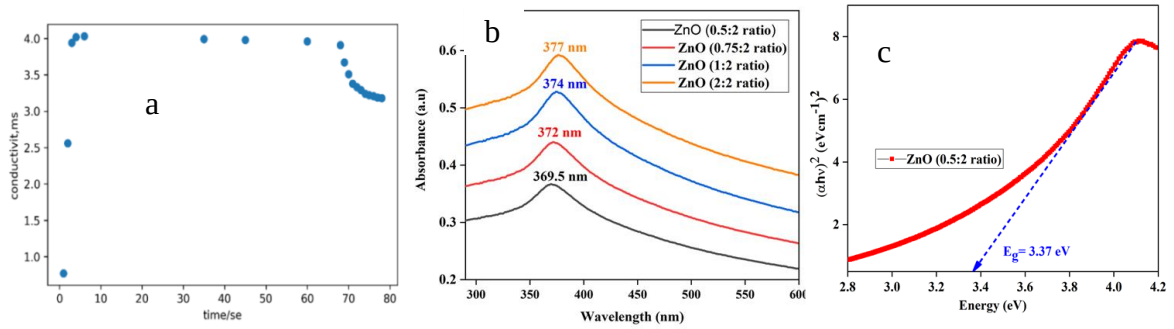

 doi:10.20944/preprints202405.0630.v2

Figure 1. a) Plot of conductivity versus time of reaction b) UV-vis spectra of the ZnO NPs synthesized using different concentrations of orange peel extract as a reducing agent and c) the Tauc plot of the ZnO NPs synthesized using a concentration of 0.25 v/v orange peel extract. .

Figure 2a-d are plots of the band gap, size, surface energy, and concentration of the ZnO NPs against the concentration of the extract utilized during the synthesis process. It is evident from the plot that an increase in the concentration of the extract leads to a reduction in the band-gap values and an increase in the size of the ZnO NPs. This phenomenon occurs as a result of the conversion of more Zn+ to Zn as the concentration of the reducing agent rises, thereby increasing the surface reaction rate. The band gap widens as the particle size decreases, since the proximity of electron-hole pairs results in a non-negligible columbic interaction, leading to heightened kinetic energy. In figure 2c, the observed increase in surface energy with increasing reducing agent concentration can be attributed to the subsequent increase in size leading to a larger surface area and ultimately a higher surface energy. The peaks on UV-vis spectra can be utilized to calculate nanoparticle concentrations via the Beer-Lambert law (equation s1). To accurately calculate the concentration as per Equation s1, it is essential to have knowledge of the molar extinction coefficient specific to the nanoparticles under consideration, see figure s7. The extinction coefficient has been determined for ZnO NPs in correlation with their particle size. The relevant data was extracted from ref[12] and it was replotted using matplotlib, (figure s2) and a mathematical correlation between the extinction coefficient and particle size was established(see equation s8). In figure 2d, the plot shows a rapid increase in the number of ZnO NPs as the concentration of the reducing agent increases from zero to 0.35 v/v, however, after 0.35 v/v, the rate of change decreases. This phenomenon can be attributed to the critical role that zinc ions and the reducing agent play in the production of zinc oxide nanoparticles. Manipulation of only one factor, such as the concentration of the reducing agent in this scenario, can significantly impact the rate of nanoparticle formation, provided that a sufficient quantity of zinc ions is available for reduction. Conversely, if the concentration of the reducing agent increases without a corresponding increase in zinc ions, there will be no significant influence on the formation rate.

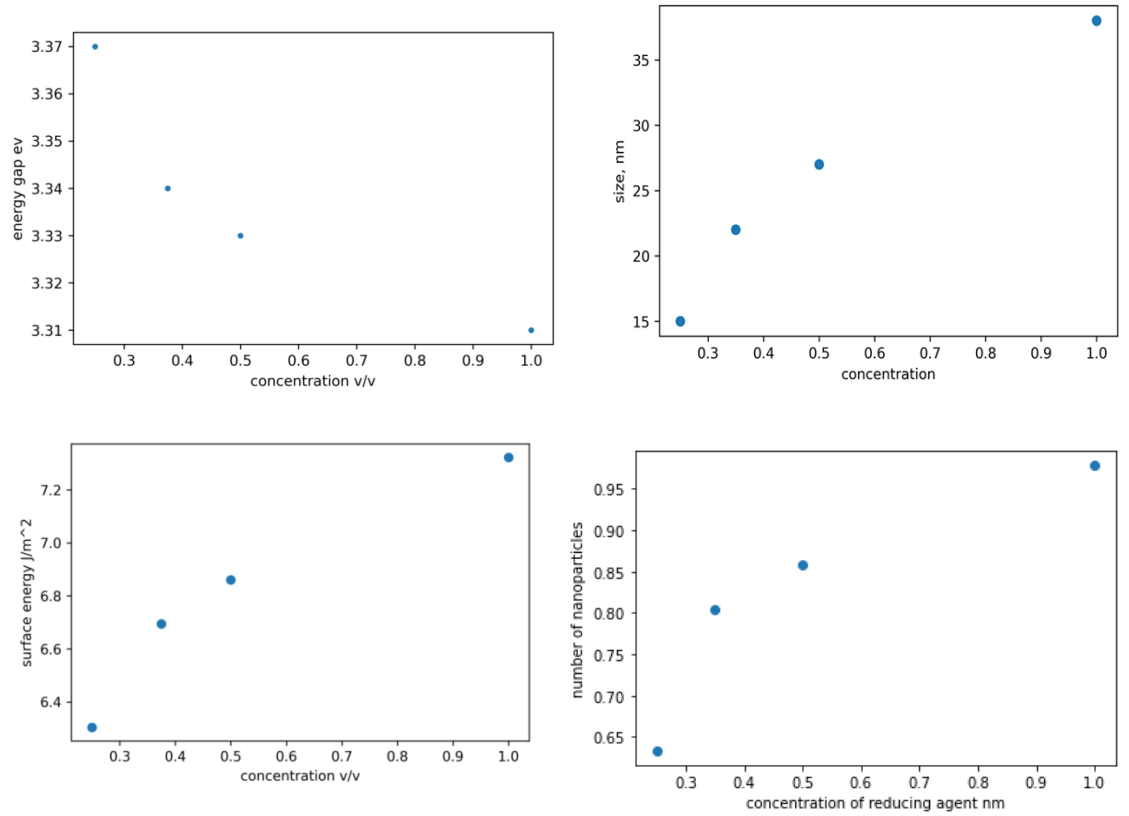

 doi:10.20944/preprints202405.0630.v2

Figure 2. a-d) plot of optical bandgap, size, surface energy, and number of ZnO NPs versus concentration of the reducing agent.

Figure 3a illustrates the FTIR spectra of ZnO NPs synthesized using varying proportions of orange peel extracts. The FTIR spectra of alcohols, phenols, or water molecules exhibit a significant peak around 3414–3442 cm^{-1} attributed to O-H stretching. Peaks within the range of 1400–1649 cm^{-1} are linked to C=O stretching, while the band at 1398 cm^{-1} is associated with the bending vibration of COH. Furthermore, Zn-OH stretching vibrations are denoted by small, intense bands at 875 cm^{-1} and 712 cm^{-1}. Figure 3b shows the XRD pattern of ZnO NPs synthesized using 0.5 v/v orange peel extract. The ZnO NP diffraction peaks were determined to be zincate phases with hexagonal wurtzite crystal structures and lattice constants of a = b = 3.248532 and c = 5.203366. The estimated average crystalline size (D) of the synthesized zinc oxide nanoparticles was found to be 19.2 nm.

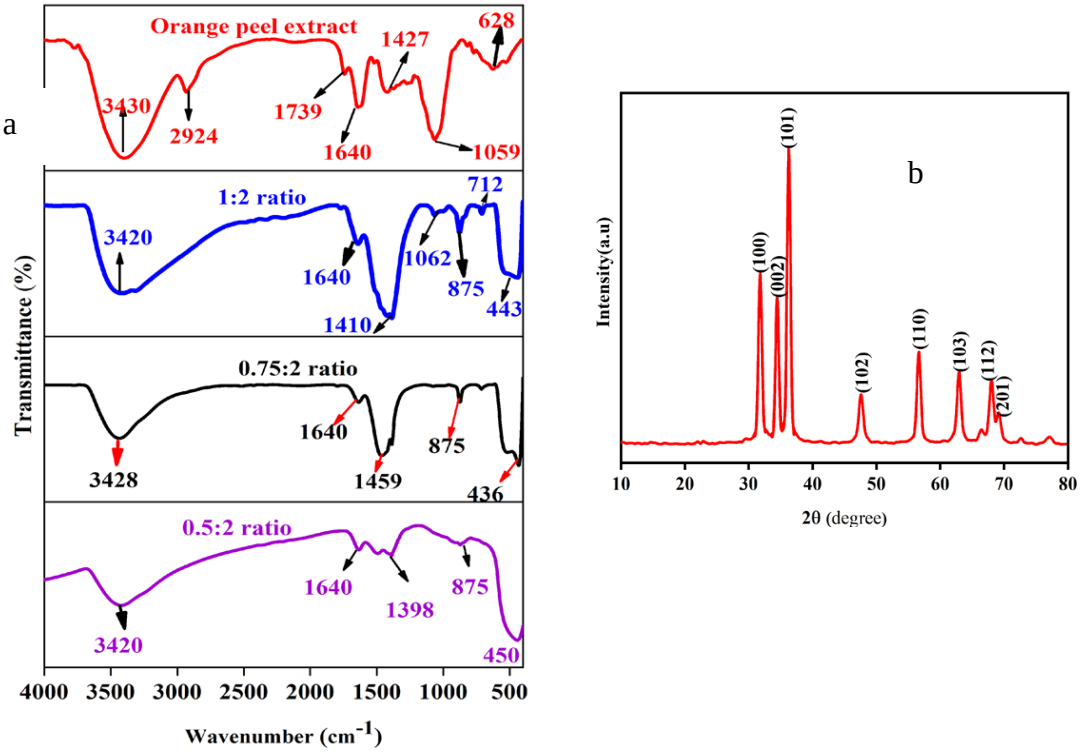

Figure 3. a) FTIR spectra of aqueous orange peel extract and ZnO NPs and b) XRD pattern of the ZnO NPs,.

The morphology of the ZnO NPs was revealed by SEM analysis, as depicted in Figure 4. The particle sizes observed in the SEM images ranged from 75 to 180 nm with an average particle size 100 nm, demonstrating consistency with prior research outcomes[13]. Discrepancies in the average particle size reported by XRD (19.2 nm) and SEM (100 nm) may be due to the extended storage duration (90 days for SEM and 10 days for XRD) before SEM analysis, which could lead to particle aggregation and coalescence. Elemental analysis was performed using energy dispersive X-ray spectroscopy **(EDX),** and the existence of zinc was confirmed by the presence of a few peaks between 1 and 10 Kev, including a significant peak at 1 keV (Figure 4b). The zinc and oxygen elements are present with a weight percentage of 83.22% and 16.78%, respectively, which is close to the bulk weight percentage of zinc oxide (80 for Zn and 20 for O). In **addition, the analysis showed atomic percentages of 54.82% for zinc and 45.18% for oxygen,** with an atomic percentage composition similar to the results reported in related studies.

 doi:10.20944/preprints202405.0630.v2

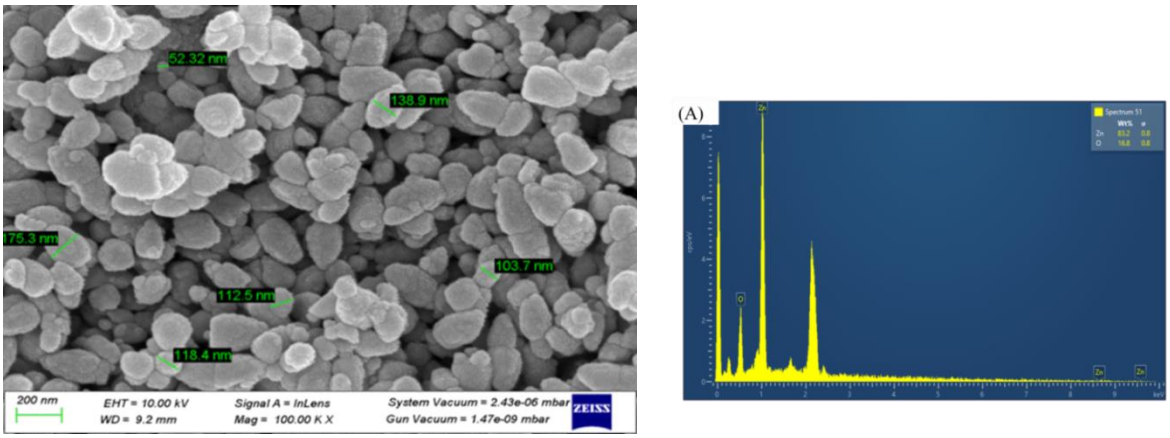

Figure 4. a) SEM image of the ZnO NPs synthesized using 0.5 v/v orange peel extract and b) elemental analysis with **EDX.**

4. Conclusions

In the present study, the observed decrease in conductivity during the synthesis process provides preliminary evidence for the reduction of zinc ions and the potential formation of ZnO NPs. UV-vis spectral analysis confirmed that the maximum absorption was in the 365 to 380 nm range, which is specific for ZnO NPs. Furthermore, the optical band-gap energies were determined from UV-vis spectroscopic data using the Tauc plot. An increase in the concentration of the reducing agent resulted in a decrease in the ZnO NPs band gap and a shift in the absorption maxima toward higher wavelengths. FTIR analysis showed characteristic peaks at 436, 443, and 450 cm^{-1}, confirming the formation of ZnO NPs. XRD analysis confirmed the hexagonal wurtzite structure of the ZnO NPs, with well-matched diffraction peaks. The SEM analysis confirmed the size and morphology of the nanoparticles. The elemental composition, elemental mapping, and purity were determined by EDX studies.

Author Contributions: E.W conducted the experimental work while G.T conceived the idea and wrote the paper.

Funding: The authors acknowledge the International Science Program (ISP), Sweden, for financial support.

Conflicts of Interest: The author declares that there are no conflicts of interest with respect to the publication of this paper.

Data Availability: The data can be obtained from the corresponding author upon request.

References

1. Osman, A. I. et al. Synthesis of Green Nanoparticles for Energy, Biomedical, Environmental, Agricultural, and Food Applications: A Review. Environmental Chemistry Letters vol. 22 (Springer International Publishing, 2024).
2. Singh, J. *et al.* 'Green' synthesis of metals and their oxide nanoparticles: Applications for environmental remediation. *J. Nanobiotechnology* **16**, 1–24 (2018).
3. Rajalakshmi, T. U. *et al.* Evidence on temperature and concentration of reducing agents to control the nanoparticles growth and their microbial inhibitory efficacy. *Mater. Res. Express* **10**, (2023).
4. Kim, H. seok *et al.* Concentration Effect of Reducing Agents on Green Synthesis of Gold Nanoparticles: Size, Morphology, and Growth Mechanism. *Nanoscale Res. Lett.* **11**, (2016).
5. Kumar, B., Smita, K., Cumbal, L. & Debut, A. Green approach for fabrication and applications of zinc oxide nanoparticles. *Bioinorg. Chem. Appl.* **2014**, (2014).
6. Toma, M., Ursulean, N., Marconi, D. & Pop, A. Structural and optical characterization of Cu doped ZnO thin films deposited by RF magnetron sputtering. **70**, 127–131 (2019).
7. Wong, E. M., Bonevich, J. E. & Searson, P. C. Growth kinetics of nanocrystalline ZnO particles from colloidal suspensions. *J. Phys. Chem. B* **102**, 7770–7775 (1998).
8. Srikant, V. & Clarke, D. R. On the optical band gap of zinc oxide. *J. Appl. Phys.* **83**, 5447–5451 (1998).
9. Mamouei, M., Budidha, K., Baishya, N., Qassem, M. & Kyriacou, P. A. An empirical investigation of deviations from the Beer–Lambert law in optical estimation of lactate. *Sci. Rep.* **11**, 1–9 (2021).

 doi:10.20944/preprints202405.0630.v2

10. Malek, F. & Nahid, M. Influence of temperature and concentration on biosynthesis and characterization of zinc oxide nanoparticles using cherry extract. *J. Nanostructure Chem.* **8**, 93–102 (2018).
11. Vollath, D., Fischer, F. D. & Holec, D. Surface energy of nanoparticles - influence of particle size and structure. *Beilstein J. Nanotechnol.* **9**, 2265–2276 (2018).
12. Chem, J. M. Light absorption by colloidal semiconductor quantum dots. 10406–10415 (2012) doi:10.1039/c2jm30760j.
13. Gaspar, D. *et al.* Ag and Sn Nanoparticles to Enhance the Near-Infrared Absorbance of a-Si:H Thin Films. *Plasmonics* **9**, 1015–1023 (2014).